Sensors and Actuators B 192 (2014) 111–116

Contents lists available at ScienceDirect

Sensors and Actuators B: Chemical

journal homepage: www.elsevier.com/locate/snb

Enhancement of detection by selective modification of silicon nanobelt field-effect transistors via localized Joule heating

Hao Heng Liu, Tzung Han Lin, Jeng-Tzong Sheu*

Institute of Nanotechnology/Materials Science and Engineering, National Chiao Tung University, 1001 Ta Hsueh Road, Hsinchu 30050, Taiwan

ARTICLE INFO

Article history:
Received 23 July 2013
Received in revised form 18 October 2013
Accepted 22 October 2013
Available online 30 October 2013

Keywords:
Methoxy-poly (ethylene-glycol)-silane
Silicon nanobelt field-effect transistor
Localized Joule heating
Selective modification
Streptavidin

ABSTRACT

We utilized localized Joule heating to ablate methoxy-poly (ethylene-glycol)-silane (mPEG-sil) modified on the p^- region of an n^+–p^-–n^+ silicon nanobelt field-effect transistor (SNFET). SNFETs with selective modifications of 3-aminopropyltrimethoxysilane (APTMS) and NHS-biotin on the ablated region exhibited a faster sensing response rate and a higher sensitivity in real-time detection of Streptavidin (SA). Characterization of the ablated region via lateral force microscopy and the fluorescence image show that the ablation region occurs only in the p^- region near the drain side and is believed to be a result of the impact ionization mechanism during Joule heating. Moreover, a bias of 20 V pulse voltage for 1 ms successfully ablates mPEG-sil and reduces the device off leakage current by 1 order after Joule heating. However, Joule heating with a pulse voltage larger than 20 V (1 ms) yielded an increase of device off leakage owing to damage to gate dielectrics during Joule heating. A comparison of real-time detection of SA between selectively and non-selectively modified chips shows that selectively modified ones exhibit a better limit of detection (LOD) that is one order lower than non-selectively modified ones, and a sensing response rate twice as fast as the non-selectively modified one for every target concentration.

1. Introduction

Silicon nanodevices, especially silicon nanowires, have been applied in the biosensing for over 10 years. These structures with high surface-to-volume ratios result in high sensitivity to changes in surface potential. Although nanowires have demonstrated the ability to detect biomarker into the subpicomolar range [1–6], sufficiently thin nanoribbons also are sensitive enough [7,8] while operating in the so-called subthreshold region [9]. Nonetheless, previous efforts in biosensing still have room for improvement. For example, sensing response rate is not fast enough when the concentration of targets is low. Simulation results have demonstrated that a faster sensing response rate can be achieved by passivation of the non-reacted regions while leaving only high sensitive regions exposed to the targets [10]. This selective modification is aimed to solve this issue by allowing specified chemical linkers or biomolecules to bind on a wanted location. Several techniques have been developed to selectively modify SAM on a silicon dioxide surface and have reported selective patterning of SAM from micro- to nanoscale [11–15]. However, all of these techniques have either simple process or accurate deposition ability, but not both. Researchers have recently developed a new technique that can carry out selective modification while combining both advantages [16]. They used the localized Joule heating to ablate the PTFE film on the silicon nanowire devices for further surface modifications. Since the heat is only confined to the silicon nanowire because it has the highest resistance in the structure, the ablated regions only occur along the silicon nanowire. However, PTFE is difficult to ablate via heat due to its high boiling point; other study has used PMMA as a passivation material and has demonstrated the same function [17]. Nonetheless, PMMA usually causes non-specific binding during real-time detection, and still requires an additional process to passivate the non-reacted regions, which may cause contamination of the modified molecules in the ablated regions when the PMMA removal process is proceeding. Another method investigated a bottom-up method for selective modification, but integrate of all processes on the chip to achieve mass production was difficult [18]. Furthermore, mPEG-sil has been employed to reduce the non-specific binding of proteins [19,20]. In this research, we simplify the selective modification process and use highly sensitive SNFET, performing localized Joule heating to selectively remove the mPEG-sil passivation layer, with subsequent modification by chemical linkers. In addition, real-time detection of SA is performed and compared for selectively and non-selectively modified chips.

* Corresponding author. Tel.: +886 3 5131491; fax: +886 3 5729910.
E-mail address: jtsheu@faculty.nctu.edu.tw (J.-T. Sheu).

0925-4005/$ – see front matter © 2013 Elsevier B.V. All rights reserved.
http://dx.doi.org/10.1016/j.snb.2013.10.102

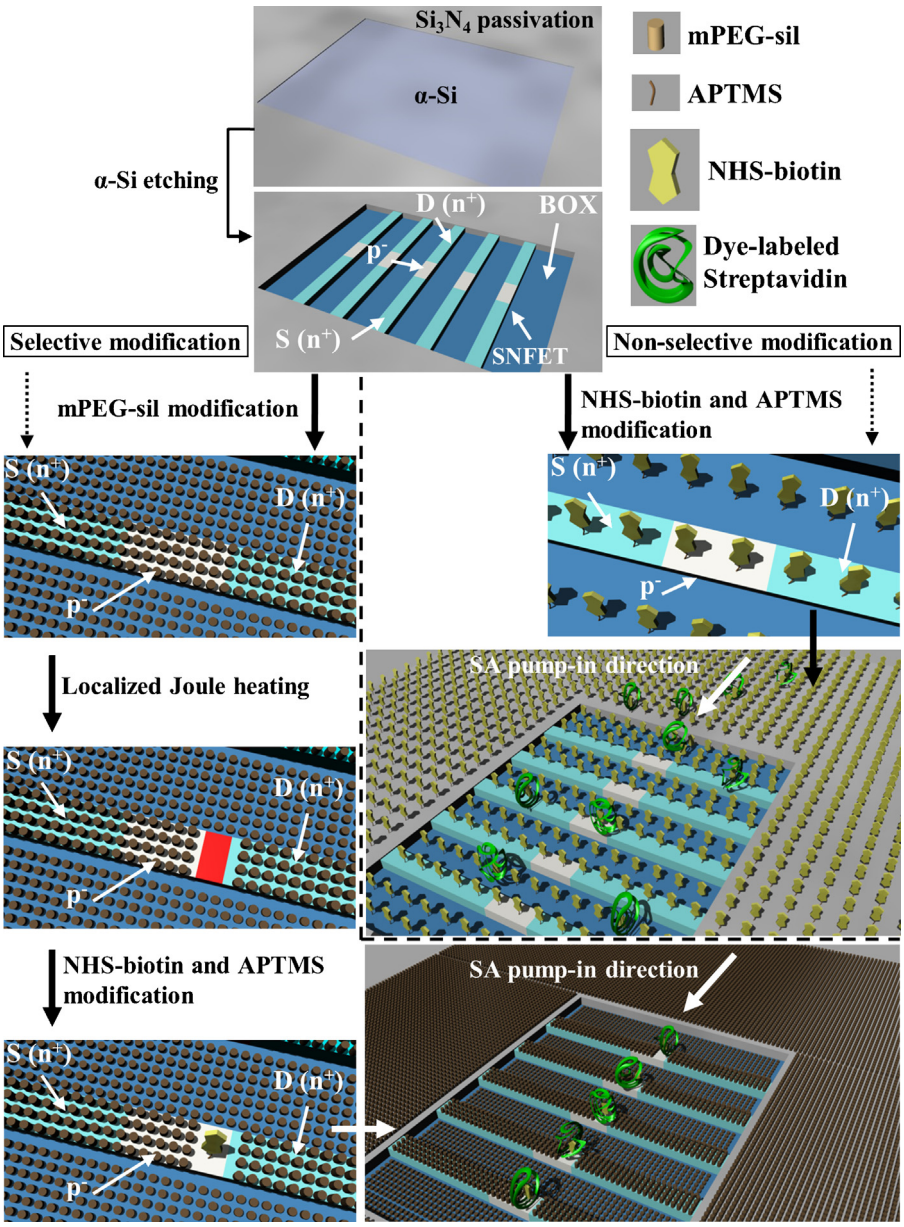

Fig. 1. Schematic diagrams showing the process of selective modification and detection of SA on SNFETs. Selective (left part) and non-selective modification (right part) processes are separated by dashed line.

2. Experimental

2.1. Device fabrication

The devices were fabricated from p-type SOI wafers with a 70-nm-thick top silicon and a 150-nm-thick buried oxide. The patterns of SNFETs were defined by photolithography using I-line stepper, and followed by Si etching via reactive ion etching (RIE). The length and width of each nanobelt is 13 μm and 500 nm, respectively. After RCA cleaning, an 8-nm-thick thermal oxide and a 100-nm-thick α-Si were grown. The contact region, which heavy doping region is also defined by photolithography and leaving a 2-μm-long intrinsic region in the middle of the nanobelts was then implanted with arsenic at a dose of 3×10^{15} cm^{-2} at 30 keV. After dopant activation, the Al-Cu alloy was deposited with a sintering process to form ohmic contact. Finally, 500-nm-thick Si_3N_4 was deposited on the devices as a passivation layer. Before modification of mPEG-sil, the α-Si layer was etched by XeF_2 isotropic silicon etching system (XACTIX). The outer Si_3N_4 layer is used as a hard mask to resist F^- attack, with the etching selectivity between Si_3N_4 and Si with XeF_2 at least 100:1. Detail fabrication processes were illustrated in the Supplementary data.

2.2. Surface modification

2.2.1. Immobilization of mPEG-sil and APTMS

SNFETs were cleaned by UV/ozone for 10 min prior to modification of mPEG-sil. The mPEG-sil (Mw = 460–590 Da) was prepared as a 6 mM mPEG-sil solution with 1% tetraethyl ammonium (TEA) as a catalyst and then reacted with the surface of chip for 24 h on a hotplate at 60 °C. After the reaction was finished, devices were cleaned sequentially with anhydrous toluene and alcohol for 5 min to remove unreacted molecules. Finally, the sample was rinsed with DI water and blown dry in a nitrogen stream. 3-aminopropyltrimethoxysilane (APTMS) (Sigma) was then deposited with a concentration of 2 mM in DI water for 10 min,

washed with DI water in an ultrasonicator three times, and blown dry by a nitrogen stream.

2.2.2. Biotin grafting and Streptavidin binding

In the case of Streptavidin binding, 1 mg of NHS-biotin powder was first dissolved in 150 μl of DMSO and then added to 850 μl of 1× PBS for a total volume of 1 ml. The NHS functional group reacted with an amino group of APTMS for 2 h. Chips were then washed by DI water and blown dry with a nitrogen stream. Finally, 10 μg/ml of Alexa Fluor® 488 Streptavidin (Invitrogen) with 0.1% Tween20 was provided onto the chips and interacted with NHS-biotin for 1 h.

2.3. Joule heating and characterization

Joule heating was carried out by an Agilent 41501B Pulse Generator Unit. Lateral force microscopy images were captured by atomic force microscopy (AFM) (DI 3000, Digital Instruments), and fluorescence images were characterized by a confocal microscope.

2.4. Electrical characterization and real-time detections

All electrical measurements were performed via an Agilent 4155B. The real-time measurements were all performed in polydimethylsiloxane (PDMS) microfluidic channels to minimize the sample amounts. PDMS is Sylgard 184 from Dow Corning, and mixed at 10:1 (w/w) with the included curing agent. It was stirred vigorously until well mixed and degassed in a vacuum chamber. Then it was poured on the premade SU8 mold and cured at 80 °C for 90 min. Finally, the hardened PDMS microfluidic channels were peeled off the mold. SA was supplied via microfluidic channel by a peristaltic pump. The gate voltage was applied via an Ag/AgCl reference electrode to manipulate the SNFET through the PBS buffer.

3. Results and discussion

Fig. 1 presents schematic diagrams of the procedures for selective and non-selective modification. The α-Si acting as a protection layer to decrease the damage on the gate oxide by the plasma during the dry etching process was etched by XeF_2 to expose the SNFET channels. The mPEG-sil was then modified on the whole device as a passivation layer. After dense mPEG-sil formation, it is ablated by localized Joule heating using a short pulse (1 ms) in vacuum (~10^{-5} torr) for the case of selective modification. Then the chemical linkers, APTMS and NHS-biotin, are modified sequentially onto the both selective and non-selective modification. Finally, the Streptavidin are supplied via the microfluidic channel to perform real-time sensing.

Fig. 2 shows the structure and transfer characteristics of the SNFETs. SNFETs were multi-channel designed for enhancement of the S/N ratio and to increase the number of binding sites, and consist of two silicon pads and five nanobelts. In addition, there are 2-μm-long intrinsic doping regions in the middle of each nanobelt; this design makes the channel conductance adjustable by the liquid gate and able to operate in the high sensitive region, the so-called subthreshold region. The subthreshold swing (SS) measured using a liquid gate is 122 mV/dec, a value sufficient for biosensing as compared to previous research [9]. The on/off ratio is five orders, implying a large dynamic sensing range.

The results of ablation of mPEG-sil are shown in Fig. 3. Because the temperature increase during localized Joule heating is much faster, we performed ablation of mPEG-sil under vacuum [21]. Unlike performing localized Joule heating on resistive nanodevices with very short duration pulse [17], the localized Joule heating for SNFET can be achieved using lower pulse voltage (15 V, 20 V, and 25 V) but need a longer duration (1 ms) in vacuum. The temperature distribution was also investigated using TCAD simulation (see

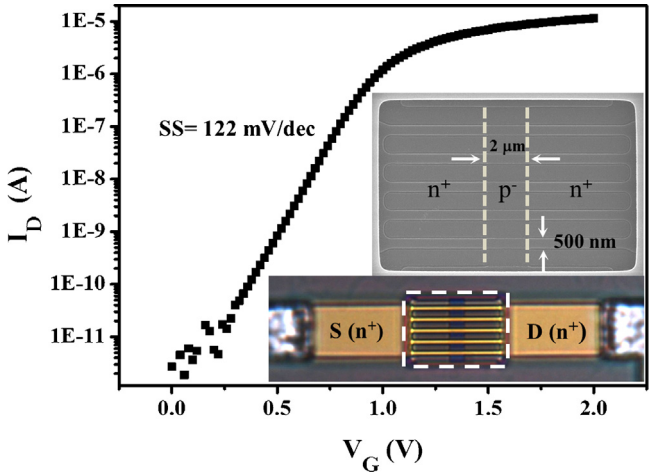

Fig. 2. The I_D–V_G characteristic of SNFETs measured via a liquid gate in the microfluidic channel. The subthreshold swing is 122 mV/dec. Insets: SEM and OM image of SNFET, with SEM taken from the region marked by dashed line block in the OM image. The doping type, source (S) and drain (D) of the SNFET are marked on SEM and OM images.

Supplementary data, Fig. S1); the results demonstrate that impact ionization occurred at the p^- region near drain side and gave rise to a sufficient temperature to remove the mPEG-sil when applied a voltage larger than 15 V. Since the height of the mPEG-sil monolayer was 1–2 nm and too short to be observed in the topography signal, LFM images are used to verify the ablation of the mPEG-sil, as shown in the left inset of Fig. 3. The LFM images were extracted from only the centermost of the five nanobelts; each image can be divided into three parts by two obvious boundaries, with the middle being the intrinsic region (marked by p^-) and other two being source and drain (marked by S and D). The location of this center nanobelt has been highlighted by two dashed lines. The length of the ablated region was extracted from the LFM image and the error bar consists of all five nanobelts. Results showed that the ablated regions of mPEG-sil expand as the pulse voltage increases; the length is 152, 266, and 412 nm, respectively, corresponding to 15-, 20- and 25-V

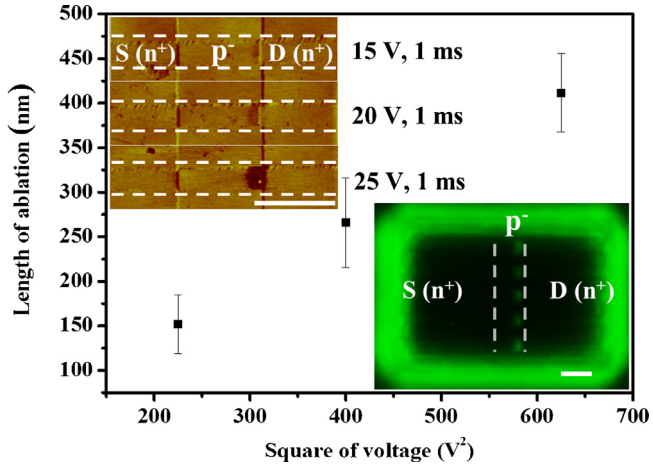

Fig. 3. The plot of length of ablation vs. square of applied voltage. White dashed lines in LFM images (left inset) highlight the location of the nanobelt. High contrast region (deep brown color in the p^- region) is defined as the ablation region and the length is extracted along the axial direction of nanobelts for all five nanobelts and for all pulse conditions. The pulse conditions are marked near the LFM images. Right inset is the fluorescence image taken after SA binding. The p^- region is highlighted by dashed lines. There are five green zones present in the p^- region and close to D. Scale bars are all 2 μm. (For interpretation of the references to color in this figure legend, the reader is referred to the web version of this article.)

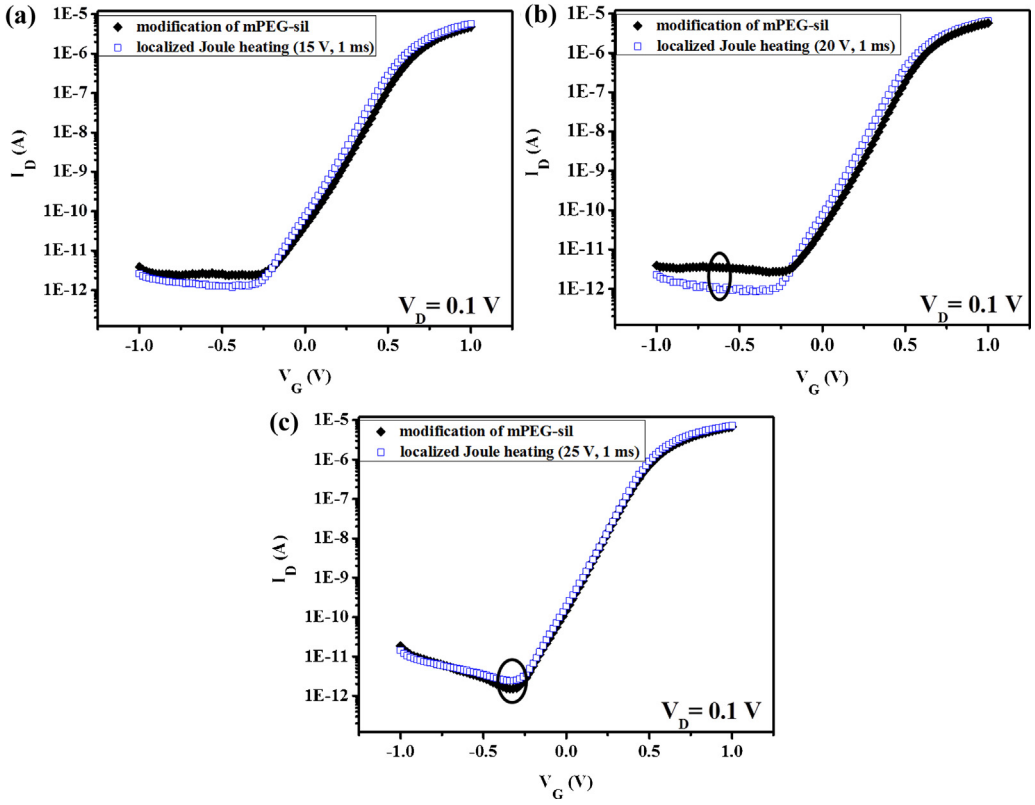

Fig. 4. The I_D–V_G characteristics before and after localized Joule heating with V_G applied by a liquid gate. Open blue rectangle (□) and solid black dimond (♦) denote the device before and after localized Joule heating, respectively. Pulse condition in (a) 15 V, 1 ms. (b) 20 V, 1 ms, with circle highlighting off-current improvement of ~1 order at −0.625 V. (c) 25 V, 1 ms, and circle highlighting off-current degradation of ~1.6 times at −0.3 V. (For interpretation of the references to color in this figure legend, the reader is referred to the web version of this article.)

pulse voltages. The ablated region is located at the intrinsic regions (p^-) and shifts to the drain side of the device. Moreover, the shift phenomenon is mainly due to the impact ionization which results from the strong horizontal electric field along the axial direction of the nanobelts during Joule heating. The right inset shows the results of the SA bound with selectively modified biotin for a 20-V pulse voltage. It is obvious that the green fluorescence spots only appear in the intrinsic regions (highlighted with two dashed lines, marked with p^-) on the five parallel nanobelts near the drain side. The fluorescence image exhibits a result consistent with the LFM images; this indicates a successfully selective modification of APTMS and NHS-biotin. On the other hand, the fluorescence intensity outside the ablated regions was almost undistinguishable, demonstrating the highly efficient passivation of the mPEG-sil layer.

Before performing the real-time measurements, the transfer characteristics of devices were examined, as shown in Fig. 4. The characteristics of devices were demonstrated by measuring the I_D–V_G curves before and after localized Joule heating. The gate voltage was applied via an Ag/AgCl reference electrode in a 10-μl drop of 0.001× PBS. Fig. 4a shows that the off-current for the case of applying 15-V pulse voltage was ca. 1×10^{-11} A at its initial state, and after localized Joule heating the off leakage current was slightly lower than at the initial state. For a 20-V pulse voltage, the off leakage current was improved by nearly one order to ca. 1×10^{-12} A, as shown in Fig. 4b. We believe that a large voltage stress for Joule heating created electron-hole pairs via impact ionization near drain, and improvement of device characteristics is most likely due to the hot-hole injection mechanism [22]. For a 25-V pulse voltage, minor Si/SiO_2 interface damage occurred at the gate/drain region by the bombardment of hot carriers under strong electric field. Therefore, the off leakage current increases a little due to trap-assisted tunneling, as shown in Fig. 4c. The leakage will cause threshold voltage drift during real-time detection, resulting in an undistinguishable threshold voltage change, even though the SNFET was not operated at negative gate bias. Moreover, the I_D–V_G curves shift parallel toward negative voltage in all cases, for the positive charges were trapped at the silicon-silicon dioxide interface caused by hot-hole injection [23]. In addition, after performing localized Joule heating at different pulse voltages, the SS remained approximately unchanged, and decaying only slightly in all cases; this implies that there are absence of deep-level traps occurring during heating (<20 V, 1 ms). Therefore, the optimized localized Joule heating condition was chosen as 20 V for lower off leakage current and larger ablated regions.

Fig. 5 shows the results of real-time SA detections. The control set was to modify the biotin on the whole chip, whereas the experimental set was to modify the biotin only in the ablated regions, with other regions passivated by mPEG-sil. The devices were operated at the subthreshold region and controlled by a liquid gate for higher sensitivity. Because of the thin gate dielectrics (10 nm) and the thick buried oxide (150 nm), the channel controllability using liquid gate is better than that using back gate. The transfer characteristics of a SNFET exhibited the efficiency using liquid gate. Moreover, even though the bottom gate sweeps at a large range (−3 to 3 V), the current response remains unchanged (see Supplementary data, Fig. S2). The 15 pM, 150 pM, and 1.5 nM of SA were introduced sequentially into the microfluidic channel at a flow rate of 48 μl/min for 20 min, and they were washed with 0.001× buffer in between SA introductions until the current change remained stable. It was found that the surface potential extracted from the transfer characteristic drops at different rates corresponding with various SA concentrations. The magnitudes of surface potential change were

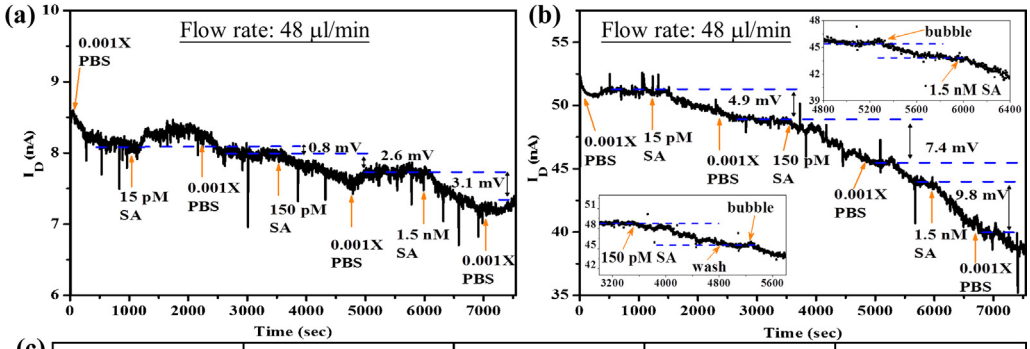

(c)

	Conditions	15 pM	150 pM	1.5 nM
Non-selective modification	Surface potential (mV)	0.8	2.6	3.1
	Sensing response rate (mV/min)	0.03	0.11	0.12
Selective modification	Surface potential (mV)	4.9	7.4	9.8
	Sensing response rate (mV/min)	0.20	0.31	0.68

Fig. 5. Real-time detection of SA. (a) Non-selective modification case and (b) selective modification case. The flow rate is 48 μl/min. The sample changing time and the surface potential change is labeled in both Figures. The left and right insets are the zoom-in plots in (b) from 3000 to 5800 s and from 4800 to 6400 s. (c) Table summarizes the surface potential and sensing response rate for case (a) and (b) at three concentrations.

defined by the differences between the stable levels before injection and after PBS wash and were 0.8 mV, 2.6 mV, and 3.1 mV for 15 pM, 150 pM, and 1.5 nM, respectively, as shown in Fig. 5a. The binding rate of SA is expected to be lower in non-selectively modified case than in selectively modified case, hence SA did not bind with biotin but within the long debye screen length (ca. 23.3 nm for 0.001× PBS) causes additional surface potential change. Therefore, the device current increase after PBS wash only happened in the non-selectively modified case. For the experimental set, the magnitudes of surface potential change were 4.9 mV, 7.4 mV, and 9.8 mV, as shown in Fig. 5b. The roll-off of device current at 5300 and 7000 s is attributed to the present of bubbles in the microfluidic channel. The bubble hinders the conduction path between reference electrode and device surface and causes the decrease of device current. However, the current maintained stable at least for 400 s after PBS wash until the bubble injected at 5300 s. We deliver the next SA concentration (1.5 nM) at 6000 s after the current maintain stable for 400 s. The potential change for 1.5 nM was estimated from the current change during 6000–6800 s. The device current maintains stable for 300 s after PBS wash and starts to drop at 7100 s. The magnitudes of potential change in these concentrations were reasonable compared to previous research [18]. The maximum change in our result is ~9.8 mV for 1.5 nM of SA, and the maximum change for the previous result was ~20 mV for 10 nM of SA. It is clear that the magnitude of surface potential change was nearly unapparent when 15-pM SA was introduced for the control set, due to the fact that the SA is trapped preferentially by the biotin which is located in front of the highly sensitive region. Since the sensitive regions are much smaller when compared with other regions, it is difficult to deliver SA to the highly sensitive region at low SA concentration. The surface potential changes slightly even if 1.5 nM of SA is introduced. In contrast, the device with mPEG-sil passivation and selective modification has a higher magnitude of surface potential change when the 15 pM SA is introduced. Although the binding sites in sensitive regions are fewer for the experimental set than for the control set, the amounts of binding SA for the experimental set are still larger than control, leading to a high sensitivity. We also examined the sensing response rate for both cases (Fig. 5c). The sensing response rate for the control set at 15 pM, 150 pM and 1.5 nM was 0.03, 0.11, and 0.12 mV/min, respectively, and for the experimental set was 0.20, 0.31, and 0.68 mV/min, respectively. These results are in good agreement with the simulation results [10]; the higher concentration of SA on the top of the high sensitive region produces the higher binding rate due to the larger driving force of concentration gradient.

4. Conclusions

Highly sensitive SNFETs have been successfully manufactured by a simple CMOS compatible process. Localized Joule heating is performed on the SNFETs and ablates mPEG-sil in the highly sensitive regions. Furthermore, the performance of the SNFET does not decay after localized Joule heating but instead improves under optimized pulse conditions (20 V, 1 ms). According to the fluorescence test results, selective modification of chemical linkers is successful; the fluorescence only appears on the ablated regions, corresponding to LFM measurement results. Finally, real-time detections show that LOD is improved by one order (420–42 pM) and the sensing response rate is at least twice as fast for all test concentrations for the selectively modified chip. This research demonstrates a simple way to achieve fast detection combined with a simple semiconductor which undergoes a selective modification process.

Acknowledgements

The authors would like to thank MOE-ATU Program and National Science Council (NSC 101-2120-M-009-011-CC1) in Taiwan for financial support.

Appendix A. Supplementary data

Supplementary data associated with this article can be found, in the online version, at http://dx.doi.org/10.1016/j.snb.2013.10.102.

References

[1] J. Hahm, C.M. Lieber, Direct ultrasensitive electrical detection of DNA and DNA sequence variations using nanowire nanosensors, Nano Lett. 4 (2004) 51–54.
[2] F. Patolsky, G. Zheng, C.M. Lieber, Nanowire sensors for medicine and the life sciences, Nanomedicine 1 (2006) 51–65.

[3] G.F. Zheng, X.P.A. Gao, C.M. Lieber, Frequency domain detection of biomolecules using silicon nanowire biosensors, Nano Lett. 10 (2010) 3179–3183.
[4] M.M.A. Hakim, M. Lombardini, K. Sun, F. Giustiniano, P.L. Roach, D.E. Davies, P.H. Howarth, M.R.R. de Planque, H. Morgan, P. Ashburn, Thin film polycrystalline silicon nanowire biosensors, Nano Lett. 12 (2012) 1868–1872.
[5] G. Shalev, G. Landman, I. Amit, Y. Rosenwaks, I. Levy, Specific and label-free femtomolar biomarker detection with an electrostatically formed nanowire biosensor, NPG Asia Mater. 5 (2013) e41.
[6] G.J. Zhang, L. Zhang, M.J. Huang, Z.H.H. Luo, G.K.I. Tay, E.J.A. Lim, T.G. Kang, Y. Chen, Silicon nanowire biosensor for highly sensitive and rapid detection of Dengue virus, Sens. Actuators B: Chem. 141 (2009) 192–199.
[7] E. Stern, J.F. Klemic, D.A. Routenberg, P.N. Wyrembak, D.B. Turner Evans, A.D. Hamilton, D.A. LaVan, T.M. Fahmy, M.A. Reed, Label-free immunodetection with CMOS-compatible semiconducting nanowires, Nature 445 (2007) 519–522.
[8] E. Stern, A. Vacic, N.K. Rajan, J.M. Criscione, J. Park, B.R. Ilic, D.J. Mooney, M.A. Reed, T.M. Fahmy, Label-free biomarker detection from whole blood, Nat. Nanotechnol. 5 (2010) 138–142.
[9] X.P.A. Gao, G.F. Zheng, C.M. Lieber, Subthreshold regime has the optimal sensitivity for nanowire FET biosensors, Nano Lett. 10 (2011) 547–552.
[10] D.R. Kim, X.L. Zheng, Numerical characterization and optimization of the microfluidics for nanowire biosensors, Nano Lett. 8 (2008) 3233–3237.
[11] N. Herzer, S. Hoeppener, U.S. Schubert, Fabrication of patterned silane based self-assembled monolayers by photolithography and surface reactions on silicon-oxide substrates, Chem. Commun. 46 (2010) 5634–5652.
[12] D.W. Wang, S.G. Thomas, K.L. Wang, Y.N. Xia, G.M. Whitesides, Nanometer scale patterning and pattern transfer on amorphous Si, crystalline Si, and SiO_2 surfaces using self-assembled monolayers, Appl. Phys. Lett. 70 (1997) 1593–1595.
[13] R.D. Piner, J. Zhu, F. Xu, S.H. Hong, C.A. Mirkin, "Dip-Pen" nanolithography, Science 283 (1999) 661–663.
[14] L. Iversen, O. Younes-Metzler, K.L. Martinez, D. Stamou, Chemically specific laser-induced patterning of alkanethiol SAMs: characterization by SEM and AFM, Langmuir 25 (2009) 12819–12824.
[15] A. George, M. Knez, G. Hlawacek, D. Hagedoorn, H.H.J. Verputten, R.V. Gastel, J.E.T. Elshof, Nanoscale patterning of organosilane molecular thin films from the gas phase and its applications: fabrication of multifunctional surfaces and large area molecular templates for site-selective material deposition, Langmuir 28 (2012) 3045–3052.
[16] I. Park, Z.Y. Li, A.P. Pisano, R.S. Williams, Selective surface functionalization of silicon nanowires via nanoscale joule heating, Nano Lett. 7 (2007) 3106–3111.
[17] C.C. Chen, Y.S. Lin, C.H. Sang, J.T. Sheu, Localized Joule heating as a mask-free technique for the local synthesis of ZnO nanowires on silicon nanodevices, Nano Lett. 11 (2011) 4736–4741.
[18] B.R. Li, C.W. Chen, W.L. Yang, T.Y. Lin, C.Y. Pan, Y.T. Chen, Biomolecular recognition with a sensitivity-enhanced nanowire transistor biosensor, Biosens. Bioelectron. 25 (2013) 452–459.
[19] M. Zhang, T. Desai, M. Ferrari, Proteins and cells on PEG immobilized silicon surfaces, Biomaterials 19 (1998) 953–960.
[20] S. Sharma, R.W. Johnson, T.A. Desai, Ultrathin poly (ethylene glycol) films for silicon-based microdevices, Appl. Surf. Sci. 206 (2003) 218–229.
[21] C.A. Santini, P.M. Vereecken, A. Volodin, G. Groeseneken, S. De Gendt, C. Van Haesendonck, A study of Joule heating-induced breakdown of carbon nanotube interconnects, Nanotechnology 22 (2011) 395202–395210.
[22] T.C. Chen, T.C. Chang, S.C. Chen, T.Y. Hsieh, F.Y. Jian, C.S. Lin, H.W. Li, M.H. Lee, J.S. Chen, C.C. Shih, Analysis of degradation mechanism in SONOS-TFT under Hot-Carrier operation, IEEE Electron Device Lett. 31 (2010) 1413–1415.
[23] B. Kim, C.K. Baek, W. Kwon, Y.H. Jeong, D.M. Kim, Simple experimental determination of the spread of trapped hot holes injected in Silicon–Oxide–Nitride–Oxide–Silicon (SONOS) cells: optimized erase and cell shrinkage, Jpn. J. Appl. Phys. 43 (2004) L1611–L1613.

Biographies

Hao Heng Liu is a Ph.D. candidate in Institute of Nanotechnology at National Chiao Tung University. He received his MS degree in Institute of Nanotechnology from National Chiao Tung University in 2006. His research interests are focusing in silicon nanodevices fabrication and applications.

Tzung Han Lin is a master student in Institute of Nanotechnology at National Chiao Tung University. He received his BS degree in Department of Chemical and Materials Engineering from National Central University in 2009. His research interests are surface modification and fabrication of silicon nanodevices.

Jeng-Tzong Sheu received the BS and the MS degrees from National Central University, JhongLi, Taiwan, in 1984 and 1986, and the Ph.D. degree in Department of Electrical Engineering from MSU, East Lansing, USA, in 1994. He joined National Nanodevice Laboratories (1994–1996) and National Synchrotron Research Center, Hsinchu, Taiwan (1996–2002) as researcher. After serving the EE Department, NCNU, Puli, Taiwan (2002–2004), he moved back to Hsinchu and served as a faculty member in the Institute of Nanotechnology, National Chiao Tung University, Hsinchu, Taiwan in August, 2004. His research interests include bridging the bottom-up and the top-down nanofabrication techniques for nanoelectronics and nanobiosensors.